Letter

One-Way Zero Reflection in an Insulator-Metal-Insulator Structure Using the Transfer Matrix Method

Heeso Noh [1] and **Jai-Min Choi [2,*]**

1   Department of Physics, Kookmin University, Seoul 02707, Korea; heesonoh@kookmin.ac.kr
2   Division of Science Education, Jeonbuk National University, Jeonju 54896, Korea
*   Correspondence: jaiminchoi@jbnu.ac.kr; Tel.: +82-63-270-2777

Abstract: We numerically demonstrate one-way zero reflection using the transfer matrix method. Using simulations, we adjusted the thickness of SiO_2 layers in a simple SiO_2-Au-SiO_2 layer structure. We found two solutions, 47 nm-10 nm-32 nm and 71 nm-10 nm-60 nm, which are the thicknesses for one-way zero reflection at a wavelength of 560 nm. We confirmed it with reflection spectra, where reflectance is zero for forwardly incident light and 2.5% for backwardly incident light at the wavelength 560 nm, and thickness 47 nm-10 nm-32 nm.

Keywords: reflection; absorption; PT-symmetry

1. Introduction

Many physical systems have a Hamiltonian with Hermitian properties, these properties lead to real and orthogonal eigenvalues. Recently Hamiltonians with parity-time (PT) symmetry have attracted a lot of interest because their eigenvalues are real below a certain threshold but are complex above that threshold [1]. PT-symmetric systems have a potential $V(\mathbf{r}) = V^*(-\mathbf{r})$. Such a system can also be realized in optics [2,3]. If the permittivity, ε, of the system has symmetry such that $\varepsilon(\mathbf{r}) = \varepsilon^*(-\mathbf{r})$, then PT-symmetry can be realized in an optical systems. Therefore, in order to satisfy PT-symmetry in optics, one should consider optical gain and loss in the system which, in turn, means ε should be represented as a complex number. This has been demonstrated many times in previous research [4–7].

One of the interesting phenomena in systems with PT-symmetry is the existence of an exceptional point. Exceptional point exists at the threshold where an eigenvalue changes from a real number to a complex number or *vice versa*. This behavior seems to be similar to that seen with degenerate states. The eigen modes, however, coalesce at an exceptional point. In other words, only one eigen mode can exist, which opens up the possibility of one-way reflection. There has been lots of research that has used this exceptional point in a variety of applications such as in single mode lasers or unidirectional reflectionlessness among others [8–13]. Recent progress in developing exceptional point-based research is well introduced in Ref. [14,15] and references therein.

Even though many physical systems use Hamiltonians to describe the physics at play, this is not the only way to describe PT-symmetry. Any kind of system can be considered, all that is required is that the PT-symmetry condition is satisfied. In optics, a scattering matrix (s-matrix) is often used to describe optical phenomena. Therefore, an s-matrix is also a candidate to describe PT-symmetric systems. One-way zero reflection has been obtained using an s-matrix in previous research [16–18]. Even though the theory for zero reflection comes from the use of an s-matrix, the reflection coefficient can be calculated with other methods. For layered structures, it is convenient to use the transfer matrix method (TMM) [19].

In this report, we use a three-layered structure that is composed of a metal layer sandwiched between two dielectric layers to obtain one-way zero reflection. We selected Au as a metal layer and SiO_2 as dielectric layers which are favored materials in photonics

research. Although there are demonstrations using Si-based structure [16,17], one-way zero reflection using the metal-based layer structure may also find its applications in various fields. By adjusting the thickness of the SiO$_2$ layers, we obtain zero reflection for forwardly incident light while we get a nonzero reflection value for backwardly incident light.

2. Simulation

Reflection and transmission were obtained using TMM for the layered structure. The electric field relation between the mth layer and the $(m+1)$th layer in the TMM is as follows.

$$
\begin{pmatrix} E_m^f \\ E_m^b \end{pmatrix} = M_m \begin{pmatrix} E_{m+1}^f \\ E_{m+1}^b \end{pmatrix},
\tag{1}
$$

$$
M_m = \begin{pmatrix} e^{-in_m k d_m} & 0 \\ 0 & e^{in_m k d_m} \end{pmatrix} \begin{pmatrix} 1/t_{m,m+1} & r_{m,m+1}/t_{m,m+1} \\ r_{m,m+1}/t_{m,m+1} & 1/t_{m,m+1} \end{pmatrix},
\tag{2}
$$

where $E_m^f(E_m^b)$ is the electric field of forwardly (backwardly) propagating light; n_m and d_m are the refractive index and thickness of the mth layer, respectly; k is the wave number in a vacuum; $r_{m,m+1}$ and $t_{m,m+1}$ are the reflection and transmission coefficients when light propagates from the mth layer to the $(m+1)$th layer. For normal incidence, the equations for $r_{m,m+1}$ and $t_{m,m+1}$ follow when relative permittivity is 1.

$$
r_{m,m+1} = \frac{n_m - n_{m+1}}{n_m + n_{m+1}}, \qquad t_{m,m+1} = \frac{2n_m}{n_m + n_{m+1}},
\tag{3}
$$

where n_{m+1} is the refractive index of the $(m+1)$th layer.

If the total number of layers is N and the electric field amplitude of incident light is 1, when the propagation direction of incident light is forward, we can write a matrix form of TMM as follows,

$$
\begin{pmatrix} 1 \\ r_f \end{pmatrix} = \begin{pmatrix} 1/t_{0,1} & r_{0,1}/t_{0,1} \\ r_{0,1}/t_{0,1} & 1/t_{0,1} \end{pmatrix} M_1 M_2 \cdots M_N \begin{pmatrix} t_f \\ 0 \end{pmatrix},
\tag{4}
$$

where r_f, t_f are the total reflection and transmission coefficients when the propagation direction of incident light is forward. When the propagation direction of incident light is backward, the relation is as follows,

$$
\begin{pmatrix} 0 \\ t_b \end{pmatrix} = \begin{pmatrix} 1/t_{0,1} & r_{0,1}/t_{0,1} \\ r_{0,1}/t_{0,1} & 1/t_{0,1} \end{pmatrix} M_1 M_2 \cdots M_N \begin{pmatrix} r_b \\ 1 \end{pmatrix}.
\tag{5}
$$

In two port system, s-matrix can be expressed as $s = \begin{pmatrix} t & r_b \\ r_f & t \end{pmatrix}$. Because PT-symmetric system maintains reciprocity, $t = t_f = t_b$. Furthermore, corresponding eignevalues are $s_n = t \pm \sqrt{r_f r_b}$. When either r_f or r_b is zero, two eigenvalues coalesce to form exceptional points, i.e., the system has one-way zero reflection.

The structure for one-way zero reflection is depicted in Figure 1a. The structure presented consists of a SiO$_2$ – Au – SiO$_2$ layers in vacuum. The thickness of the gold is fixed at 10 nm. The reason for this is that Au is highly reflective in the visible wavelength range. If the thickness of Au is too high, we cannot achieve coupling between the light in the top SiO$_2$ layer and that in the bottom SiO$_2$ layer. On the other hand, if the thickness of the Au is too low, we will no longer be able to achieve a continuous film with the Au. The Au of 10 nm thickness is right above the percolation threshold [20]. The thicknesses of the top and bottom SiO$_2$ layers are denoted by d_1 and d_2, respectively. We adjusted d_1 and d_2 to achieve one-way zero reflection. The incident light from the left is denoted as forwardly incident light; the incident light from the right, backwardly incident light.
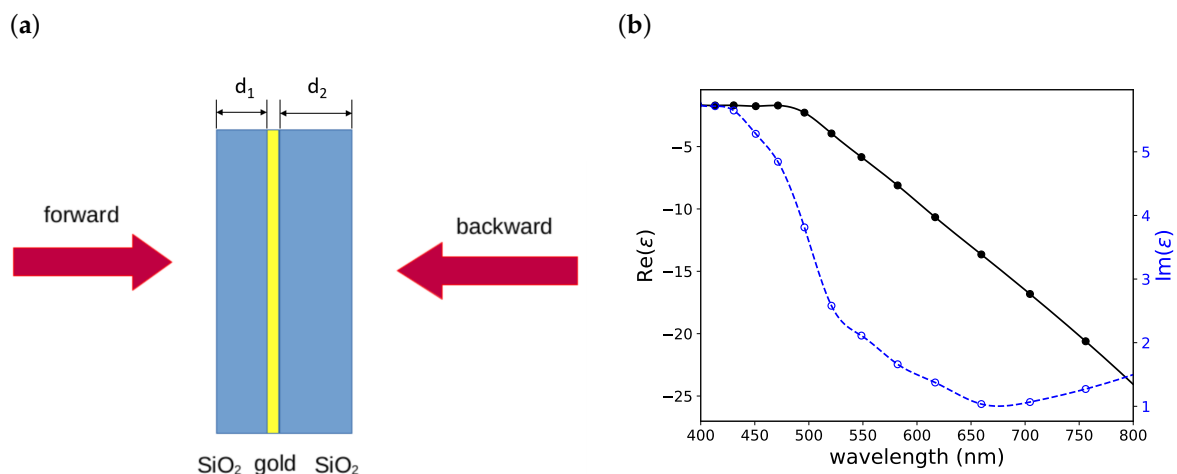
Figure 1. (**a**) Schematic of simulated structure. The three layers seen here are SiO_2-Au-SiO_2. We fixed the thickness of Au as 10 nm, and d_1 and d_2 are varied to achieve one-way zero reflection. Incident light coming from the left (right) is denoted as forwardly (backwardly) incident light. (**b**) dispersion curve of Au. The data points marked with the black filled circles (●) and the blue open circles (○) are from Ref. [21]. Solid and dashed curves are lines of best fit. The black curves represents the real part of ε, the blue curves represents the imaginary part of ε.

The relative permittivity, ε, is defined as $\varepsilon = \sqrt{n}$. The ε of SiO_2 is 2.13. As the permittivity of Au is strongly dispersive, its value changing with wavelength is not negligible so one fixed value cannot be used for a range of wavelengths. We used ε of Au from Ref. [21]. Figure 1b shows the dispersion of ε as a function of wavelength. Blue represents the real part of ε; black represents the imaginary part of ε. The data points marked with the filled circles (●) and the open circles (○) come from the reference, while the solid and dashed curves come from interpolation with the spline method. The real part of ε is negative because Au is a metal.

r_f and r_b are generally represented with complex numbers. Therefore, one can write r_f and r_b in terms of amplitude and phase. Using phase gives a great advantage when one is trying to find a zero for r_f. As such, it is possible to find where $r_f = 0$ by simply observing the phase of r_f because there will be a 2π phase change around the value zero [22]. We continuously adjusted d_1 and d_2 from 20 nm to 100 nm to find the phases of r_f and r_b.

Figures 2a,b show the false color images of the phases of r_f and r_b respectively, when the wavelength λ of the incident light is 560 nm. The colors indicate the phases of r_f and r_b. One can see that the phase changes by 2π, i.e., the color changes from the darkest blue to the darkest red, if we move counterclockwise around the bottom-left point $\mathbf{P}_1 = (47$ nm, 32 nm) of the dark line and around the top-right point $\mathbf{P}_2 = (71$ nm, 60 nm) of the dark line, where the first and second numbers correspond to d_1 and d_2, respectively. Therefore, we can see that r_f becomes zero at $\mathbf{P}_1$ and $\mathbf{P}_2$. r_b, however, does not go to zero at $\mathbf{P}_1$ and $\mathbf{P}_2$ because there is no 2π phase change around those points in false color image in Figure 2b. This indicates that one-way zero reflection has been realized at these points. It is also possible to get more accurate values for d_1 and d_2 by increasing the resolution of the false color image; this can be done by decreasing the scanning step, i.e., by reducing the interval we increment d_1 and d_2 while creating these false color image. Note that r_b goes to zero at $\mathbf{P}_1^T = (32$ nm, 47 nm) and $\mathbf{P}_2^T = (60$ nm, 71 nm), where $\mathbf{P}_1^T$ ($\mathbf{P}_2^T$) is transposed of $\mathbf{P}_1$ ($\mathbf{P}_2$). This is because the Au layer is embedded with the two SiO_2 layers.

(**a**) (**b**)
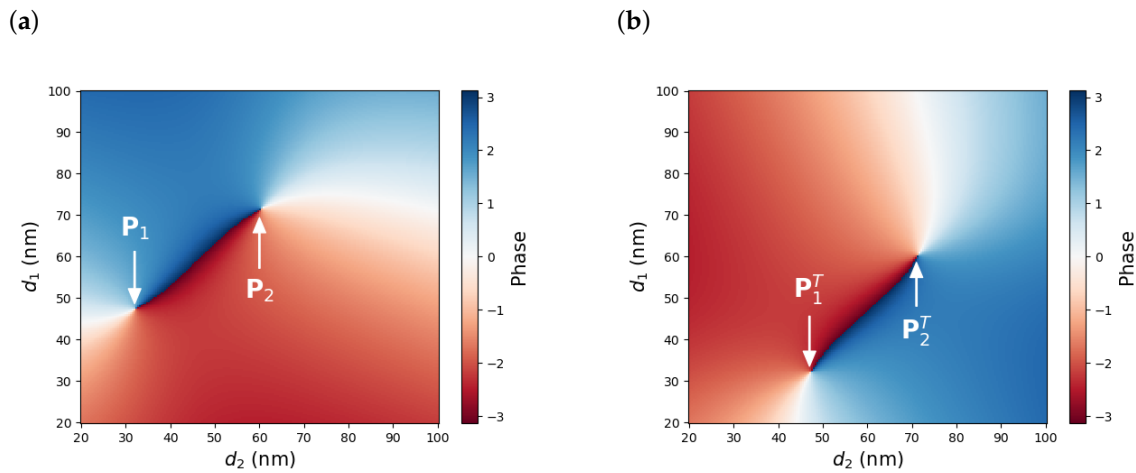
Figure 2. The false color image showing the phases of r_f(a) and r_b(b). (**a**) $r_f = 0$ at $\mathbf{P}_1 =$ (47 nm, 32 nm) and $\mathbf{P}_2 =$ (71 nm, 60 nm) because a phase change of 2π occurs around these points. (**b**) $r_b = 0$ at $\mathbf{P}_1^T =$ (32 nm, 47 nm) and $\mathbf{P}_2^T =$ (60 nm, 71 nm), where the first and second numbers correspond to d_1 and d_2, respectively.

3. Results and Discussion

In order to confirm one-way zero reflection, we calculated the reflectance of the simulated structures: SiO_2(32 nm)-Au(10 nm)-SiO_2(47 nm) and SiO_2(60 nm)-Au(10 nm)-SiO_2(71 nm). Reflectance is defined as the square of the absolute value of the reflection coefficient. Therefore, with forwardly incident light the reflectance is $|r_f|^2$, for backwardly incident light it is $|r_b|^2$. Figure 3a shows the reflectance as a function of wavelength for $d_1 = 32$ nm and $d_2 = 47$ nm. The blue solid curve is for the reflectance of forwardly incident light, the black dashed curve is for the reflectance of backwardly incident light. The numerically calculated reflectance is less than 10^{-5} for forwardly incident light while it is not zero but 2.5% for backwardly incident light at $\lambda = 560$ nm. These results confirm that we have one-way zero reflection at $\lambda = 560$ nm, which agrees with our simulation results presented in Figure 2. Figure 3b shows the transmittances of $|t_f|^2$ ($|t_b|^2$) for forwardly (backwardly) incident light. The blue solid curve shows the transmittance of forwardly incident light; the black dashed curve shows the transmittance of backwardly incident light. The blue solid and black dashed curves overlap exactly, which means the transmittance for forwardly incident light is the same as for backwardly incident light.

(**a**) (**b**)
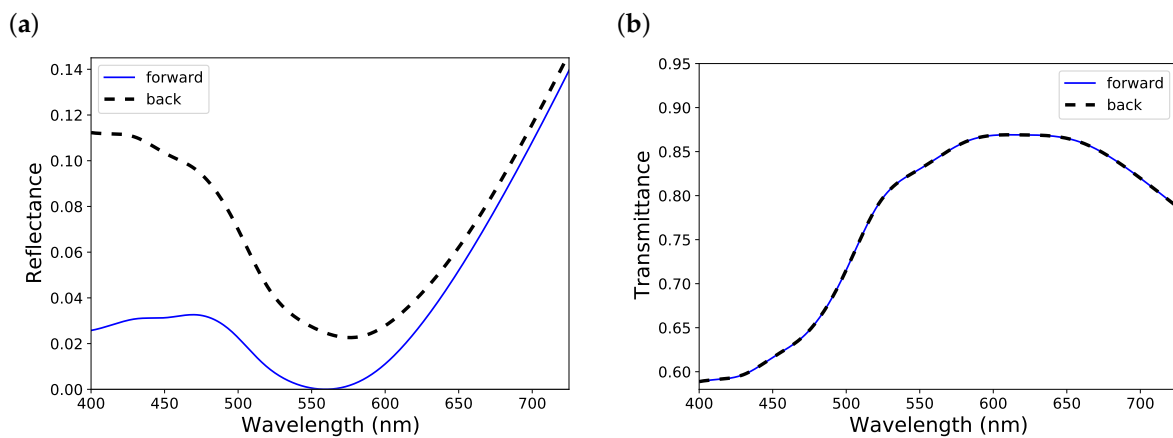
Figure 3. Reflectance and transmittance for a structure with $d_1 = 32$ nm and $d_2 = 47$ nm (**a**) Reflectance of forwardly incident light (blue solid curve) and backwardly incident light (black dashed curve) as a function of wavelength. Only reflectance of forwardly incident light becomes zero at $\lambda = 560$ nm. (**b**) Transmittance of forwardly incident light (blue solid curve) and backwardly incident light (black dashed curve) as a function of wavelength. The transmittance is the same for both forwardly and backwardly incident light.

Figure 4a shows the reflectance as a function of wavelength for $d_1 = 60$ nm and $d_2 = 71$ nm. The blue solid curve shows the reflectance of forwardly incident light; the black dashed curve shows the reflectance of backwardly incident light. The numerically calculated reflectance is less that 10^{-5} for forwardly incident light while it is not zero but 1.4% for backwardly incident light at $\lambda = 560$ nm. These results confirm that we achieve one-way zero reflection at $\lambda = 560$ nm. Figure 4b shows the transmittance. The blue solid curve shows the transmittance of forwardly incident light, the black dashed curve shows the transmittance of backwardly incident light. The blue solid and black dashed curves overlaps exactly.

The reflectance and transmittance results indicate that the absorption is different for forwardly and backwardly incident light because $Reflectance + Transmittance + Absorption = 1$. Figure 5 shows the absorption spectra of forwardly incident light (blue solid curve) and backwardly incident light (black dashed curve) as a function of wavelength for $d_1 = 47$ nm and $d_2 = 32$ nm (a), $d_1 = 60$ nm and $d_2 = 71$ nm (b). In both cases, absorption is higher for forwardly incident light compared to backwardly incident light.
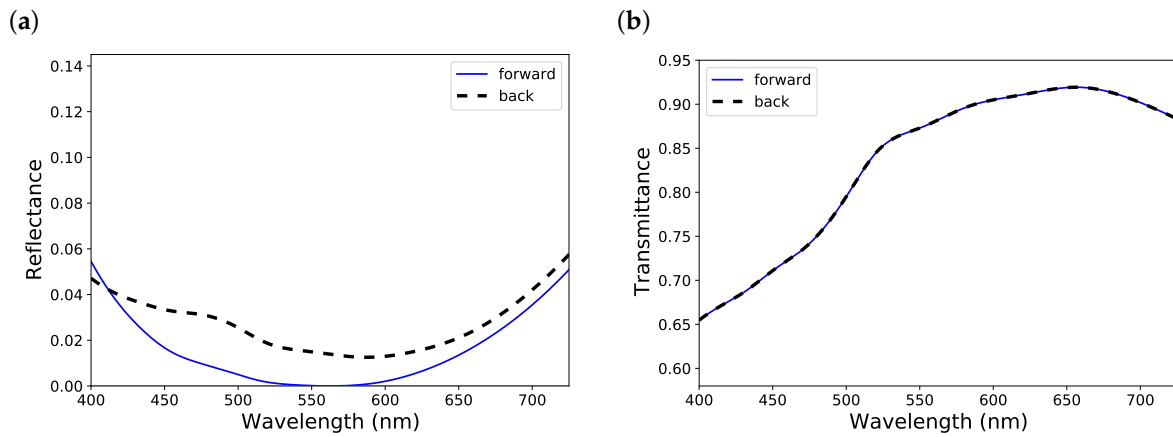
Figure 4. Reflectance and transmittance for a structure with $d_1 = 60$ nm and $d_2 = 71$ nm (**a**) Reflectance of forwardly incident light (blue solid curve) and backwardly incident light (black dashed curve) as a function of wavelength. Only the reflectance of forwardly incident light becomes zero at $\lambda = 560$ nm. (**b**) Transmittance of forwardly incident light (blue solid curve) and backwardly incident light (black dashed curve) as a function of wavelength. The transmittance is the same for both forwardly and backwardly incident light.
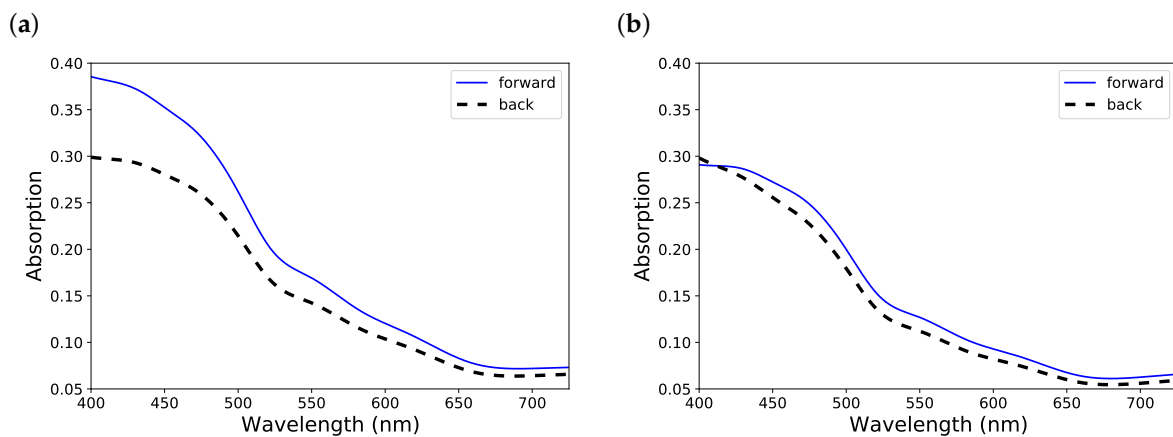
Figure 5. Absorption spectra of forwardly incident light (blue solid curve) and backwardly incident light (black dashed curve) as a function of wavelength for a structure with $d_1 = 47$ nm and $d_2 = 32$ nm (**a**), $d_1 = 60$ nm and $d_2 = 71$ nm (**b**).

4. Conclusions

We used TMM to simulate one-way zero reflection through an insulator-metal-insulator (IMI) structure. We used SiO_2 for the two outer insulator layers and Au for the middle metal layer. By examining a range of thicknesses for both the SiO_2 layers with the 10-nm Au layer at $\lambda = 560$ nm, we found two pairs of thicknesses that produced one-way zero reflection: $d_1 = 47$ nm (60 nm) for the top layer and $d_2 = 32$ nm (71 nm) for the bottom layer. We also confirmed one-way zero reflection using reflectance spectra. The reflectance becomes zero for forwardly incident light, while it is not zero for backwardly incident light. The reflectance of backwardly incident light is higher when $d_1 = 47$ nm and $d_2 = 32$ nm compared to when $d_1 = 60$ nm and $d_2 = 71$ nm.

Even though we used a metal as the absorption material, any material with absorption could be used to achieve one-way zero reflection, such as silicon demonstrated in prior research with various configurations [16,17]. IMI structure proposed in the context of one-way zero reflection may be adapted in optical fiber-based biosensors to investigate the possible increase of light coupling to the sensing region [23]. One-way zero reflection has great potential when applied in systems where no reflection is important, such as in solar cells.

Institutional Review Board Statement: Not applicable.

Informed Consent Statement: Not applicable.

Conflicts of Interest: The authors declare no conflict of interest.

References

1. Bender, C.M.; Boettcher, S. Real Spectra in Non-Hermitian Hamiltonians Having PT Symmetry. *Phys. Rev. Lett.* **1998**, *80*, 5243–5246. [CrossRef]
2. Longhi, S.; Della Valle, G. Photonic Realization of PT-Symmetric Quantum Field Theories. *Phys. Rev. A* **2012**, *85*, 012112. [CrossRef]
3. Bender, C.M. Making Sense of Non-Hermitian Hamiltonians. *Rep. Prog. Phys.* **2007**, *70*, 947–1018. [CrossRef]
4. Musslimani, Z.H.; Makris, K.G.; El-Ganainy, R.; Christodoulides, D.N. Optical Solitons in PT Periodic Potentials. *Phys. Rev. Lett.* **2008**, *100*, 030402. [CrossRef] [PubMed]
5. Guo, A.; Salamo, G. J.; Duchesne, D.; Morandotti, R.; Volatier-Ravat, M.; Aimez, V.; Siviloglou, G.A.; Christodoulides, D.N. Observation of PT-Symmetry Breaking in Complex Optical Potentials. *Phys. Rev. Lett.* **2009**, *103*, 093902. [CrossRef] [PubMed]
6. Rüter, C.E.; Makris, K.G.; El-Ganainy, R.; Christodoulides, D.N.; Segev, M.; Kip, D. Observation of Parity-Time Symmetry in Optics. *Nat. Phys.* **2010**, *6*, 192–195. [CrossRef]
7. Miri, M.-A.; LiKamWa, P.; Christodoulides, D.N. Large Area Single-Mode Parity–Time-Symmetric Laser Amplifiers. *Opt. Lett.* **2012**, *37*, 764. [CrossRef]
8. Lin, Z.; Ramezani, H.; Eichelkraut, T.; Kottos, T.; Cao, H.; Christodoulides, D.N. Unidirectional Invisibility Induced by PT-Symmetric Periodic Structures. *Phys. Rev. Lett.* **2011**, *106*, 213901. [CrossRef]
9. Liertzer, M.; Ge, L.; Cerjan, A.; Stone, A.D.; Türeci, H.E.; Rotter, S. Pump-Induced Exceptional Points in Lasers. *Phys. Rev. Lett.* **2012**, *108*, 173901. [CrossRef]
10. Feng, L.; Xu, Y.L.; Fegadolli, W.S.; Lu, M.H.; Oliveira, J.E.B.; Almeida, V.R.; Chen, Y.F.; Scherer, A. Experimental Demonstration of a Unidirectional Reflectionless Parity-Time Metamaterial at Optical Frequencies. *Nat. Mater.* **2013**, *12*, 108–113. [CrossRef]
11. Brandstetter, M.; Liertzer, M.; Deutsch, C.; Klang, P.; Schöberl, J.; Türeci, H.E.; Strasser, G.; Unterrainer, K.; Rotter, S. Reversing the Pump Dependence of a Laser at an Exceptional Point. *Nat. Commun.* **2014**, *5*, 4034. [CrossRef] [PubMed]
12. Feng, L.; Wong, Z.J.; Ma, R.M.; Wang, Y.; Zhang, X. Single-Mode Laser by Parity-Time Symmetry Breaking. *Science* **2014**, *346*, 972–975. [CrossRef] [PubMed]
13. Hodaei, H.; Miri, M.A.; Hassan, A.U.; Hayenga, W.E.; Heinrich, M.; Christodoulides, D.N.; Khajavikhan, M. Parity-Time-Symmetric Coupled Microring Lasers Operating around an Exceptional Point. *Opt. Lett.* **2015**, *40*, 4955. [CrossRef] [PubMed]
14. Miri, M.-A.; Alú, A. Exceptional points in optics and photonics. *Science* **2019**, *363*, eaar7709. [CrossRef]
15. Wiersig, J. Review of exceptional point-based sensors. *Photonics Res.* **2020**, *8*, 1457–1467. [CrossRef]

16. Shen, Y.; Deng, X.H.; Chen, L. Unidirectional Invisibility in a Two-Layer Non-PT-Symmetric Slab. *Opt. Express* **2014**, *22*, 19440. [CrossRef]
17. Feng, L.; Zhu, X.; Yang, S.; Zhu, H.; Zhang, P.; Yin, X.; Wang, Y.; Zhang, X. Demonstration of a Large-Scale Optical Exceptional Point Structure. *Opt. Express* **2014**, *22*, 1760. [CrossRef]
18. Huang, Y.; Veronis, G.; Min, C. Unidirectional Reflectionless Propagation in Plasmonic Waveguide-Cavity Systems at Exceptional Points. *Opt. Express* **2015**, *23*, 29882. [CrossRef]
19. Na, J.; Noh, H. Investigation of a Broadband Coherent Perfect Absorber in a Multi-Layer Structure by Using the Transfer Matrix Method. *J. Korean Phys. Soc.* **2018**, *72*, 66–70. [CrossRef]
20. Ducourtieux, S.; Podolskiy, V.A.; Grésillon, S.; Buil, S.; Berini, B.; Gadenne, P.; Boccara, A.C.; Rivoal, J.C.; Bragg, W.D.; Banerjee, K.; et al. Near-Field Optical Studies of Semicontinuous Metal Films. *Phys. Rev. B* **2001**, *64*, 1654031–16540314. [CrossRef]
21. Johnson, P.B.; Christy, R.W. Optical Constants of the Noble Metals. *Phys. Rev. B* **1972**, *6*, 4370–4379. [CrossRef]
22. Andreasen, J.; Vanneste, C.; Ge, L.; Cao, H. Effects of Spatially Nonuniform Gain on Lasing Modes in Weakly Scattering Random Systems. *Phys. Rev. A* **2010**, *81*, 043818. [CrossRef]
23. González-Vila, Á.; Debliquy, M.; Lahem, D.; Zhang C.; Mégret, P.; Caucheteur, C. Molecularly imprinted electropolymerization on a metal-coated optical fiber for gas sensing application. *Sens. Actuators B Chem.* **2017**, *244*, 1145–1151. [CrossRef]